Elucidating an amorphous form stabilization mechanism of tenapanor hydrochloride: crystal structure analysis using Xray diffraction, NMR crystallography and molecular modelling

Article

Accepted Version

Elucidating an Amorphous Form Stabilization Mechanism of Tenapanor Hydrochloride: Crystal Structure Analysis using X-ray Diffraction, NMR Crystallography and Molecular Modelling

Sten O. Nilsson Lill*[a], Cory M. Widdifield[b†], Anna Pettersen[a], Anna Svensk Ankarberg[c], Maria Lindkvist[c], Peter Aldred[c], Sandra Gracin[c], Norman Shankland[d], Kenneth Shankland[d,e], Staffan Schantz[c], and Lyndon Emsley*[f]

AUTHOR ADDRESS [a] Pharmaceutical Sciences, IMED Biotech Unit, AstraZeneca Gothenburg, SE-431 83, Mölndal, Sweden. [b] Institut des Sciences Analytiques (CNRS/ENS de Lyon/UCB Lyon 1), Centre de RMN à Très Hauts Champs, Université de Lyon, 69100 Villeurbanne, France. [c] Pharmaceutical Technology & Development, AstraZeneca Gothenburg, SE-431 83, Mölndal, Sweden. [d] CrystallografX Ltd, 2 Stewart Street, Milngavie, Glasgow G62 6BW, United Kingdom. [e] School of Pharmacy, University of Reading, Whiteknights, P.O. Box 224, Reading, RG6 6AD, United Kingdom. [f] Institut des Sciences Ingénierie Chimiques, Ecole Polytechnique Fédérale de Lausanne (EPFL), CH-1015 Lausanne, Switzerland.

KEYWORDS. Amorphous, Crystal structure, Density functional theory, Solid-state NMR, Stabilization, X-ray diffraction

ABSTRACT: By the combined use of powder and single crystal X-ray diffraction, solid-state NMR, and molecular modelling, the crystal structures of two systems containing the unusually large tenapanor drug molecule have been determined: the free form, **ANHY** and a dihydrochloride salt form, **2HCl**. Dynamic nuclear polarization (DNP) assisted solid-state NMR (SSNMR) crystallography investigations were found essential for the final assignment, and were used to validate the crystal structure of **ANHY**. From the structural informatics analysis of **ANHY** and **2HCl**, conformational ring differences in one part of the molecule were observed which influences the relative orientation of a methyl group on a ring nitrogen and thereby impacts the crystallizability of the dihydrochloride salt. From quantum chemistry calculations, the dynamics between different ring conformations in tenapanor is predicted to be fast. Addition of HCl to tenapanor results in general in a mixture of protonated ring conformers and hence a statistical mix of diastereoisomers which builds up the amorphous form, **a-2HCl**. This was qualitatively verified by ^{13}C CP/MAS NMR investigations of the amorphous form. Thus, to form any significant amount of the crystalline material **2HCl**, which originates from the minor (i.e., energetically less stable) ring conformations, one needs to involve nitrogen deprotonation to allow exchange between minor and major conformations of **ANHY** in solution. Thus, by controlling the solution pH value to well below the pK_a of **ANHY**, the equilibrium between **ANHY** and **2HCl** can be controlled and by this mechanism the crystallization of **2HCl** can be avoided and the amorphous form of the dichloride salt can therefore be stabilized.

Introduction

Drugs are often marketed with the active compound being in a crystalline form.[1] However, due to issues related to slow dissolution rates, or solubility-limited drug absorption, one may need to introduce a different solid form with altered properties.[2] Amorphous forms are highly desired, as they generally offer improved solubility. The number of drugs on the market taking advantage of these desirable amorphous form properties is increasing, and is likely to further increase since poor water solubility has been raised as one of the major challenges when developing new pharmaceuticals.[3] Amorphous forms of a material may potentially be accessed by processing methods such as spray drying;[4] however, amorphous forms are generally higher in energy compared to corresponding crystalline forms, and therefore significant effort is typically required to ascertain how the amorphous form may be initially stabilized to avoid crystallization.

Herein, we describe a study on crystalline and amorphous forms containing tenapanor (systematic name: *N,N'*-(10,17-dioxo-3,6,21,24-tetraoxa-9,11,16,18-tetraazahexacosane-1,26-diyl)bis{3-[(*4S*)-6,8-dichloro-2-methyl-1,2,3,4-tetrahydroisoquinolin-4-yl]benzenesulfonamide}, Figure 1), which is currently in advanced-stage drug development by the innovator company, Ardelyx Inc. Tenapanor is being developed for the treatment of irritable bowel syndrome with constipation (IBS-C), and for the treatment of hyperphosphatemia for patients with end-stage renal disease (ESRD) on hemodialysis.[5] Further, tenapanor effectively and specifically inhibits the sodium-transporter membrane protein NHE3 in the gastrointestinal tract, thereby reducing sodium absorption in the body.[6] Today, ESRD patients are treated with phosphate binders, but safety and tolerability have been significant concerns. IBS-C is a gastrointestinal (GI) disorder in which abdominal pain or discomfort is associated with constipation, which significantly affects the health and quality of life of people living with these conditions. Therefore, there is a substantial demand for new drug products in both areas.

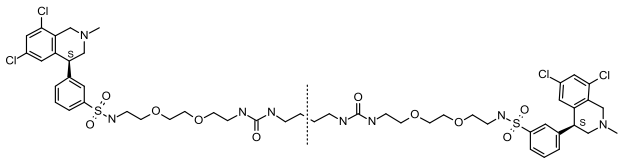

Figure 1. Molecular structure of tenapanor. Note the pseudo-mirror plane of symmetry (indicated with a dashed line) which relates the left and right-hand 'sides' of the molecule.

Precise structural information of small molecular organics can often be obtained by performing single-crystal X-ray diffraction (scXRD) experiments. However, this requires the preparation of a suitable crystal. If a suitable single crystal cannot be isolated, but rather only a microcrystalline powder sample can be obtained, powder diffraction techniques can be applied, but the resulting structural solutions are of relatively lower resolution compared to scXRD. However, it is not uncommon in modern drug development to fail to isolate even a microcrystalline powder. Compounds containing large and/or very flexible molecules may limit the possibilities for structure determination using powder diffraction data, as a large number of conformational degrees of freedom make the structure solution process more challenging.[7] When samples do not possess translational or other sufficient forms of order, diffraction techniques are less informative and local techniques such as nuclear magnetic resonance (NMR) may be applied to establish some structural information.[8]

For crystalline materials, recent advances in solid-state modelling *via* density functional theory (DFT) have led to increases in accuracy and efficiency. DFT methods can be used to produce virtual polymorph landscapes, and together with experimental techniques, provides information that can be used to evaluate the possibility that a given compound might form more stable polymorphs than the ones already observed.[9] Quantum chemistry tools can also be used to yield detailed structural information about a drug substance, and in particular how a solid-state form is stabilized.[10,11]

The present study was carried out on systems containing tenapanor (Figure 1). One system is a crystalline anhydrous form (**ANHY**), whose structure was determined using scXRD data. Other forms are composed of the dihydrochloride salt of tenapanor, which was typically produced as an amorphous powder **(a-2HCl)**. However, after extensive screening, conditions were found such that a microcrystalline powder could be obtained (**2HCl**). This crystalline form was subjected to powder XRD (PXRD) and subsequent data analysis to arrive at a refined structural solution. Complementary solid-state NMR (SSNMR) experiments were performed (^{1}H, ^{13}C, and ^{15}N), and chemical shift (δ) information was measured. Crystal structure predictions (CSP) were carried out to investigate the polymorph landscapes for **ANHY** and **2HCl**. The diffraction structures were also subjected to magnetic shielding (i.e. chemical shift) tensor calculations. Using the experimental and computed chemical shifts (and other relevant information), we attempt to assign the observed SSNMR signals to chemical sites in the tenapanor molecule(s), and perform a root-mean-squared deviation (RMSD) calculation to compare the experimental and calculated chemical shift results in the case of **ANHY**. By combining results from XRD, NMR, molecular modelling and CSP, and by connecting the structural information from experimental determinations with predictions on conformational preferences and dynamics, a stabilization mechanism which controls the formation of **a-2HCl** is presented.

Experimental

A. Solid-State Nuclear Magnetic Resonance

Most SSNMR experiments were performed at or near room temperature (T = 285 – 298 K) using Bruker AVANCE III spectrometers operating at applied magnetic field strengths (B_0) of 11.75 or 16.4 T. Experiments were also performed at T = 270 K to see if small temperature changes produced significant changes in the NMR observables. Experiments at 16.4 T used a 3.2 mm HCN triple-resonance probe to allow for reasonably rapid magic-angle spinning (MAS) rates and to enhance chemical shift dispersion, while at B_0 = 11.75 T, a 4.0 mm HX double-resonance probe was used to increase experimental sensitivity (relative to a 3.2 mm probe or a triple-resonance probe). For 'fast-MAS' ^{1}H NMR experiments, where the MAS frequency, ν_{MAS}, was ca. 60 kHz, a 1.3 mm HX double-resonance probe was used. For fast-MAS experiments, frictional rotor heating of about +26 K was measured using the temperature-dependent T_1 and chemical shift values of KBr (^{79}Br)[12] and corrected prior to formal experiments by passing chilled N_2 gas (99%) through the probe. The ^{1}H pulse length calibrations and chemical shift referencing were established with powdered adamantane (δ_{iso}(^{1}H) = 1.87 ppm) under ca. 10 – 15 kHz MAS and T = 295 – 298 K. Adamantane was also used for ^{13}C pulse calibrations, establishing ^{1}H/^{13}C cross-polarization (CP)/MAS conditions, and referencing carbon chemical shifts (with the high-frequency peak of adamantane occurring at 38.48 ppm). Uniformly ^{13}C and ^{15}N labeled glycine under ca. 6 kHz MAS and ambient temperature was typically used to set the ^{15}N chemical shift referencing (such that the observed shift of glycine is –347.54 ppm),[13] and was used to optimize ^{1}H/^{15}N CP/MAS conditions. On one occasion at B_0 = 11.75 T, ^{15}N labeled alanine was used to set the shift reference (δ_{iso}(^{15}N, alanine) ≈ −338.3 ppm). For the comparison of methyl group environments in **ANHY**, **2HCl**, and **a-2HCl** (*vide infra*), spectra were recorded at room temperature on a Bruker AVANCE III widebore spectrometer (B_0 = 9.40 T) using a 4.0 mm HX double-resonance probe. The recycle delay was set to 10 s, ν_{MAS} = 15 kHz, and CP was carried out using a linear amplitude ramp during 2 ms. Glycine was used as a secondary chemical shift reference (δ_{iso}(^{13}C, carbonyl) = 176.03 ppm).

For **ANHY** only, dynamic nuclear polarization (DNP)-enhanced SSNMR methods were applied in some situations.[14-17] Due to the very strong ^{13}C NMR signal associated with the typical DNP biradical solvent (i.e., d_8-glycerol), ^{13}C-depleted (99.95 % in ^{12}C) and fully ^{2}H-labelled glycerol was purchased from Cambridge Isotope Laboratories, Inc. The biradical polarizing agent AMUPol (Scheme S1),[18] was chosen due to its compatibility in aqueous mixtures and superior DNP performance.[19-21] DNP-enhanced SSNMR experiments were performed between T = 95 – 104 K, with the slight temperature variation due to sample heating which results from either increased MAS frequencies or increased gyrotron microwave output power. However, once a set of experimental DNP conditions was established, variation in the measured temperature over the course of the experiment was typically <3 K. DNP-enhanced SSNMR experiments were performed at B_0 = 9.4 T (AVANCE III HD console), used a 3.2 mm triple-resonance

HXY probe, sapphire rotors with PTFE inserts (to prevent solvent escape), and zirconia caps.

B. Quantum Chemical Calculations (Periodic)

Calculations under periodic boundary conditions were performed using version 5.5 of the Cambridge Serial Total Energy Package (CASTEP).[22] Input files were generated using Materials Studio (Dassault Systèmes) starting from experimental crystal structures. For all tasks (i.e. geometry optimizations, or the calculation of magnetic resonance parameters using NMR-CASTEP[23,24]), the generalized gradient approximation (GGA) DFT exchange-correlation (XC) functional of Perdew, Burke, and Ernzerhof (PBE)[25,26] was used. Core electrons were modeled with ultrasoft pseudopotentials that were generated on-the-fly. Valence electrons were described using a plane wave basis, with a typical kinetic energy cutoff of 700 eV, as this value has been widely tested and shown to be appropriate for organics.[27,28] Reciprocal space sampling of the Brillouin zone used a fixed *k*-point spacing of 0.05 $Å^{-1}$. Unit cells were fixed to the experimentally determined cell parameters, and the dispersion correction of Tkatchenko and Scheffler (TS) was always applied.[29] Self-consistent field (SCF) energy minimizations were performed until a threshold of 1×10^{-5} eV/atom was reached, and H-atom geometry optimizations continued until the total energy converged to 5×10^{-6} eV/atom with a maximum ionic force of 1×10^{-2} eV/Å. When possible/relevant, lattice symmetry was used to increase calculation efficiency.

C. Crystal Structure Prediction (CSP)

To generate a polymorph landscape for **2HCl**, the molecular conformation determined using powder XRD data (*vide infra*) was subjected to CSP methods using the Solid State Prediction Tool (SSPT) force-field developed in-house,[9,30,31] and by employing the GRACE packing machinery under $Z' = 1$ conditions.[32] The polymorph space was searched *via* a Monte-Carlo (MC) parallel tempering method followed by a lattice energy minimization for each polymorph. The generation of new trial crystal structures was continued until the convergence criterion (set to 0.7) was met. As such, we expect to have achieved a 70% probability of finding all possible solutions given the space group constraints and Z'. In all CSP runs, a large number of trial crystal structures were generated in the seven most common chiral space groups (i.e. $P2_1$, $P1$, $P2_12_12_1$, $C2$, $P2_12_12$, $P4_3$, and $C222_1$). We applied a rigid conformational polymorph search, *i.e.*, the molecular conformer was not allowed to adopt changes once in the crystal structure lattice. In addition to the experimental conformer, we also tested CSP for a series of diastereoisomeric conformers (*vide infra*) of **2HCl** differing in either the dichlorotetrahydroisoquinoline ring conformations or in the stereochemistry at the nitrogen atoms. These ring conformers were pre-optimized using the OPLS2005 force-field,[33] as implemented in MacroModel (Schrödinger Inc.), while ensuring that the core of the molecule remained fixed. Single point DFT calculations using CASTEP, employing the PBE functional and Grimme's D2 dispersion correction[34] with an energy cutoff at 600 eV, were performed on the top 60 candidates for different combinations of nitrogen stereochemistry and ring conformation (with the methyl group in either the axial or equatorial position). The 20 most stable crystal structures generated, covering a larger sphere of the tenapanor polymorph landscape, were then subjected to periodic DFT optimizations and the top 8 of these to further GIPAW magnetic shielding calculations. The NMR results were analyzed using MagresView.[35]

D. Quantum Chemical Calculations (Molecular)

Molecular model systems were optimized using M06/6-31+G(d,p)[36] as implemented in Jaguar 8.4.[37] M06 was chosen due to its well established performance for systems involving hydrogen bonds and dispersion interactions, as well as the accurate calculation of activation barriers.[38] Stationary points were characterized as minima or transition states by the sign of the eigenvalue of the Hessian matrix obtained from a frequency calculation. System Cartesian coordinates and energies can be found in the Supporting Information.

E. Powder X-ray Diffraction

The crystal structure of **2HCl** was determined from fixed count time synchrotron PXRD data collected on Beamline I11 at Diamond Light Source Ltd. [λ = 1.03482 Å, zero point = 0.009401(2)°]. Data were collected in the range $2\theta = 2 – 25.1°$. The sample was held at a temperature of 100 K in a spinning 1 mm borosilicate glass capillary. The diffraction pattern indexed to a monoclinic unit cell [M(20) = 33.4, F(20) = 198.4; DICVOL04] and $P2_1$ was deemed to be the most probable space group compatible with the presence of a single enantiomer in a unit cell of volume 2939.6 $Å^3$. Pawley refinement of the cell (conventional setting) using TOPAS (2 – 25.1° 2θ; ca. 2.4 Å) yielded an $R_{wp} = 2.83$ and zero error = -0.0128(9). To solve the structure using the simulated annealing (SA) approach implemented in DASH,[39] an input molecular model with accurate covalent bond lengths and angles, known chirality and ring conformations was derived from the **ANHY** scXRD structure. With 33 optimizable torsion angles, **2HCl** is the most complex $Z' = 1$ structure that our research groups have investigated to date. Based on the similarity of the **ANHY** and **2HCl** unit cells, we used angular constraints to bias the search towards structure solutions with torsion angles similar to those observed in the **ANHY** scXRD structure. To further improve the chances of obtaining a structure solution, we employed a very large number of SA runs (ca. 2 400, requiring a total of ca. 50 days of CPU time). Results from exploratory SA runs were used to identify the most likely aliphatic ring conformations. The best SA solution gave an $R_{wp} = 5.22$, less than a factor of two greater than Pawley $R_{wp} = 2.83$, suggesting that a good solution had been obtained. A Rietveld refinement of this structure, treating the cation as a series of rigid bodies connected by rotatable torsion angles and allowing the cation position, orientation and conformation, together with chloride ion positions, to refine, reduced the R_{wp} to 4.67. A CASTEP optimization of the refined structure, with fixed cell dimensions, gave an energy-optimized structure with a $RMSD_{15}$ value of 0.204 Å relative to the refined structure, confirming the essential correctness of the latter.[40] The crystal structure has been deposited in the Cambridge Structural Database (CSD), reference: 1576662.

F. Single-crystal X-ray Diffraction

A single colorless blade-shaped crystal of **ANHY** was obtained by slow crystallization from MeOH. A suitable crystal of 0.13 × 0.03 × 0.02 mm was selected and mounted on a MITIGEN

holder with silicon oil on a Rigaku AFC$_{12}$ FRE-VHF diffractometer equipped with an Oxford Cryostream low-temperature apparatus. The crystal was kept at T = 100(2) K during data collection. Data were measured using profile data from ω-scans of 1.0° per frame for 10.0 s using MoK$_\alpha$ radiation (rotating anode, 45.0 kV, 55.0 mA). The total number of runs and images was based on the strategy calculated from the program CrystalClear.[41] The achieved resolution was θ = 25.242. Cell parameters were retrieved and refined using the CrysAlisPro[42] software and corrected for Lorentz polarization. Completeness was 97.5% out to 25.242 in θ. The absorption coefficient (mm^{-1}) of this material is 0.365, with minimum and maximum transmissions of 0.914 and 1.000, respectively. The structure was solved by direct methods using SHELXS,[43] and refined by least squares using a version of SHELXL2012.[44] The crystal structure determined under the above conditions is provided as part of the Supporting Information and has been deposited in the CSD, reference: 1576661.

G. Solution Nuclear Magnetic Resonance

^{1}H and ^{13}C NMR spectra were acquired at 400 MHz and 100 MHz, respectively, for 30 mg/mL solutions of **2HCl** dissolved in DMSO-d_6 (see Table S1 and Figure S1 in the Supporting Information). Spectra were referenced to the signal of residual solvent (δ_{iso}(^{1}H) = 2.49 ppm, δ_{iso}(^{13}C) = 39.5 ppm).

Results and Discussion

A. Diffraction and Discussion of ANHY Structure

The crystal structure of **ANHY** was determined at T = 100(2) K using single-crystal XRD (Figure 2a). There is one symmetry-independent molecule in the unit cell (Z' = 1), and the structure does not possess any apparent voids. The overall shape of the molecular conformation is helix-like with the two terminal ends aligned in parallel. The two central urea moieties form a global hydrogen bond network, both with an NH-group in the sulfonamide, and in a bifurcated manner with another urea group (Figure 2b). There are two urea groups appearing in the tenapanor molecule which feature some differences in the strength of their hydrogen bonds, as observed from the hydrogen bond distances. The overall hydrogen bond network in the crystal structure grows in two dimensions forming sheets. Further, it is noted that the phenyl ring next to the sulfonamide group orients itself such that two CH-π interactions with two urea groups are created (Figure 2b). In addition, there exists a stabilizing halogen bond interaction between two chlorines (see Supporting Information, Figure S2). These atoms are separated by 3.27 Å, which is shorter than the sum of the vdW-radii of two independent chlorines (3.5 Å).[45]

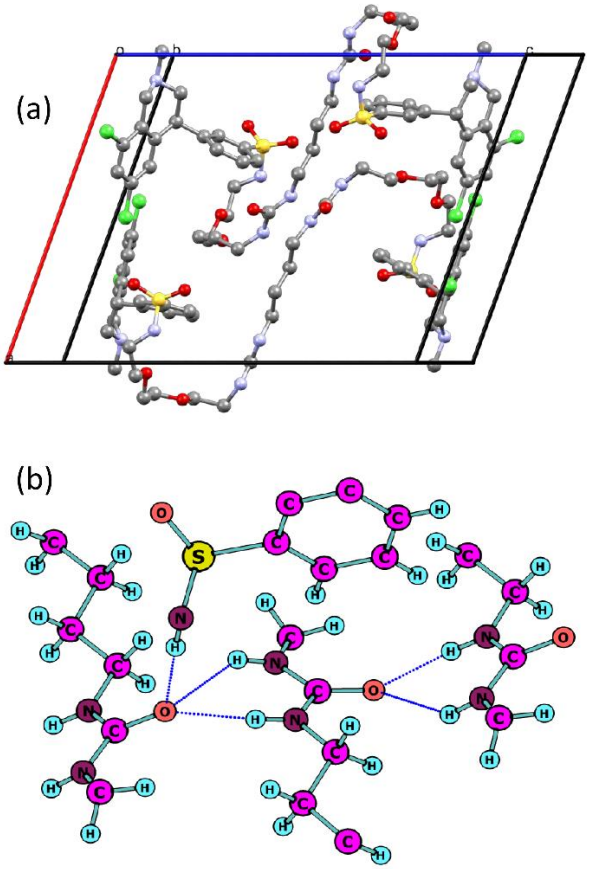

Figure 2. a) Crystal structure of **ANHY**, determined from scXRD data. Unit cell dimensions: a = 15.739 Å, b = 8.7991 Å, c = 20.589 Å, $\alpha = \gamma = 90°$, β = 110.600°, Z' = 1, Z = 2. H atoms have been omitted for clarity. b) Crystal structure extract highlighting the hydrogen bonding network involving the urea groups.

The methylated dichlorotetrahydroisoquinoline rings found at both ends of the tenapanor molecule in **ANHY** possess interesting features. The methyl group attached to each nitrogen is positioned equatorially; however, the nitrogen lone-pairs are oriented differently: in one of the six-membered rings, the nitrogen lone-pair dipole vector should be found roughly parallel to the C3-H bond, while in the other ring it should be oriented approximately anti-parallel (Figure 3 and Figure S3, see also Figure S1 for the labelling scheme used). This suggests an inversion has occurred at one of the nitrogen atoms, together with a ring-flip in the six-membered ring. DFT calculations on a model system revealed an activation barrier for this process at the M06/6-31+G(d,p) level of theory of 7–8 kcal mol^{-1}. The rate constant associated with this process is thus approximately 1 × 10^7 s^{-1}, and will be rapid *via* a conformer with the methyl substituent in the axial position (Figures 3 and 4).

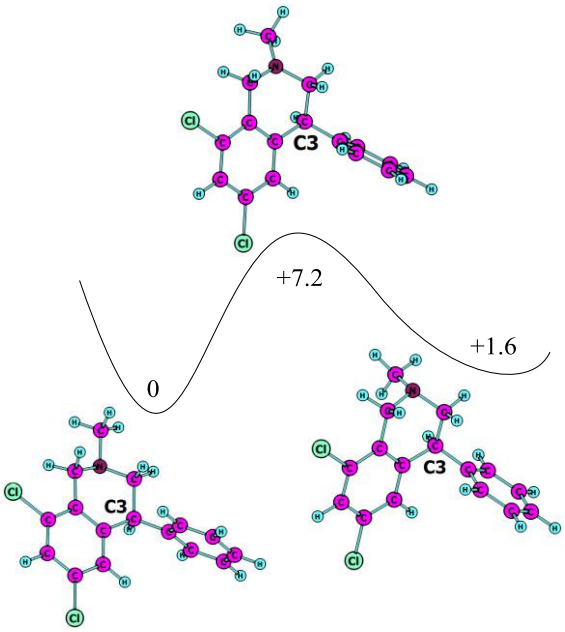

Figure 3. Schematic view of the activation process for nitrogen inversion between isomers with the methyl group attached to the nitrogen in the equatorial (left) and axial positions (right), respectively. Energies (in kcal mol^{-1}) calculated at the M06/6-31+G(d,p) level of theory are indicated.

The overall thermodynamic cycle relating the above ring conformers in **ANHY** suggests a fast dynamic equilibrium exists amongst them. Later, discussions will be provided on how this impacts the structure and crystallization of **2HCl**.

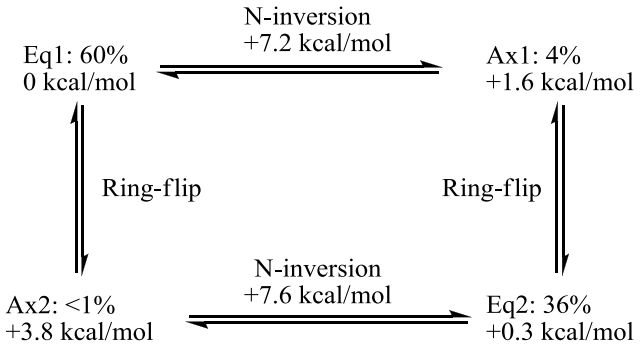

Figure 4. M06/6-31+G(d,p) calculated energies and populations for the conversion between different axial (Ax) and equatorial (Eq) conformers.

B. Solid-State Nuclear Magnetic Resonance on ANHY

In an effort to verify[46,47] the crystal structure of **ANHY**, various SSNMR experiments and quantum chemical calculations were performed. The approach used here lies within the realm of "NMR crystallography" methods which have shown great promise.[48-52] Typical ^{1}H MAS spectra (B_0 = 11.75 and 16.4 T), as well as a T_1(^{1}H) build-up curve, can be found in Figures S4 and S5, respectively. Fast ^{1}H MAS NMR experiments enabled accurate and precise measurements of several ^{1}H chemical shifts (Figure 5). The ^{1}H NMR experiments were also performed as a function of MAS frequency (4.85 – 60.32 kHz), and under static (i.e. non-spinning) conditions (Figure S6).

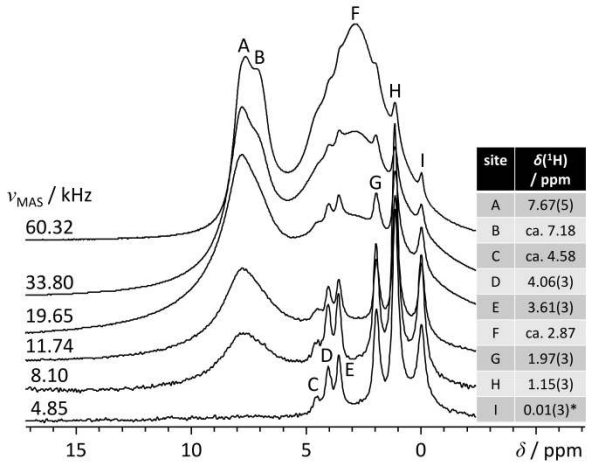

Figure 5. ^{1}H MAS SSNMR spectra of **ANHY**, acquired at B_0 = 11.75 T and with a variable MAS frequency. Spectra were acquired using a recycle delay of 15 s, and 16 transients were averaged. Site 'I' is not observed in any other ^{1}H NMR spectrum for this material, and hence possibly corresponds to an impurity phase.

Variation in the ^{1}H MAS SSNMR spectra as a function of ν_{MAS} provides evidence that the ^{1}H-^{1}H dipolar coupling network is weak. It is thus reasonable to assume that segments of the tenapanor molecule in **ANHY** undergo local dynamic motions. Local motions result in increased ^{1}H T_2* values, which in turn are consistent with the somewhat sharp spectral features that are observed for some sites at relatively modest ν_{MAS}. Even under static conditions, the "dynamic" region of the molecule is clearly present in the ^{1}H SSNMR spectrum (Figure S6, bottom), while ^{1}H signals associated with the more rigid regions of the molecule (including and near the aromatic rings) are not observed.

1D ^{13}C CP/MAS NMR experiments at B_0 = 11.75 and 16.4 T using multiple MAS frequencies resolved 35 unique ^{13}C chemical shifts for **ANHY** (Figures S7 – S9; Table S2). Spectral editing experiments[53] were also performed (Figure S10), and tentative group assignments made (Table S3). Nitrogen-15 CP/MAS NMR experiments resolved 6 nitrogen sites (Figure S11), which is fewer than the 8 expected when considering the crystal structure. Integration of the ^{15}N NMR signals establishes that the signal intensity is distributed roughly as 1:1:2:2:0.5:0.5. Upon considering the expected ^{15}N chemical shift values associated with each chemical site (confirmed with GIPAW DFT calculations, *vide infra*), it is clear that the most shielded ^{15}N signals correspond to N atoms in the rings. Less efficient ^{1}H → ^{15}N CP/MAS dynamics would be expected for these environments as: (i) they are not protonated and (ii) their nearest ^{1}H polarization sources are Me groups, where polarization buildup is relatively inefficient.

Using the above 1D SSNMR experiments, a full assignment could not be achieved. Two-dimensional (2D) heteronuclear correlation (HETCOR) experiments (^{1}H-^{13}C and ^{1}H-^{15}N) were thus performed, and enabled a more complete assignment. The resulting spectra are provided in the SI (Figures S12-S15 for ^{1}H-

^{13}C, Figure S16 for ^{1}H-^{15}N). Connectivity data, group assignments, and δ_{iso}(^{1}H) for protons attached to ^{15}N are supplied in Tables S4 – S5. In a similar fashion to what was done in a recent study on a relatively large organic molecule with potential pharmaceutical applications,[46] 2D ^{13}C-^{13}C correlation experiments were performed on **ANHY** to further complete the assignment. This included a magic-angle turning (MAT) experiment[54-56] to measure ^{13}C chemical shift tensors, and ^{13}C-^{13}C INADEQUATE NMR experiments[57,58] to clarify the carbon-carbon connectivity. Due to the very low sensitivity of the INADEQUATE experiment, DNP was used.

To briefly rationalize the MAT experiments, we note that while most are familiar with δ_{iso}, a more complete representation of nuclear magnetic shielding is given using a second-rank tensor.[59] The shielding interaction depends on the orientation between B_0 and the microcrystalline domains in the powder sample. Experimentally, a 'powder pattern' is recorded for each chemical site, with each exhibiting three characteristic break points under static (i.e., non-spinning) conditions (see Figure S17). Measurement of the full shift tensor thus increases the information for each chemical site, leading to a more robust assignment. Further MAT discussion is in the SI, with the MAT NMR spectrum of **ANHY** in Figure S18, and the measured ^{13}C shift tensor parameters in Table S6.

A typical DNP-enhanced ^{1}H MAS NMR spectrum for a sample containing **ANHY** can be found in Figure S19b. This is compared to a 'traditional' ^{1}H MAS NMR spectrum (Figure S19a) under the same experimental conditions (except with the gyrotron in standby mode). Similar measurements were performed for ^{13}C (Figure S20). The measured ^{13}C DNP enhancement factor was ca. 20 after optimization of biradical/solvent conditions.

Two DNP-enhanced ^{13}C-^{13}C INADEQUATE NMR spectra were acquired for **ANHY**, and each displays numerous correlations. The two experiments differed in their indirect dimension evolution times (i.e., t_1 lengths). This allows for greater confidence when assigning the observed ^{13}C signals to sites in the tenapanor molecule of **ANHY**. Several ^{13}C-^{13}C INADEQUATE spectra are provided (Figures 6, S21, and S22), and assigned where possible. As DFT results aided in the assignment process, the DFT frame was used to denote the site labels. A full specification of the labels is provided in Figure S23.

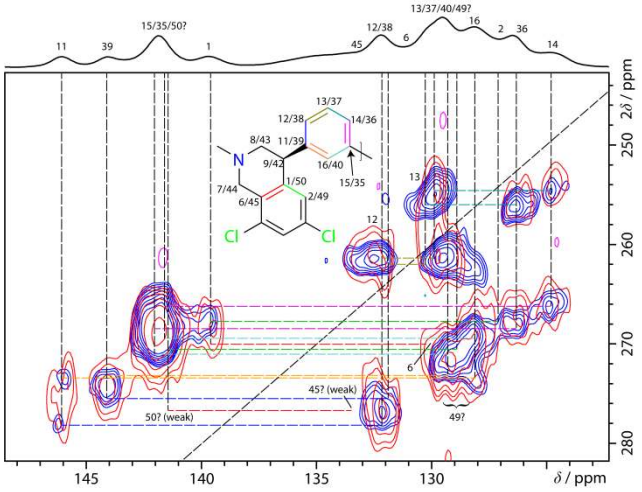

Figure 6. High-frequency region of the DNP-enhanced ^{13}C-^{13}C INADEQUATE SSNMR spectra acquired for **ANHY** at B_0 = 9.4 T, $T \approx 96$ K, ν_{MAS} = 11.0 kHz, and a ^{1}H/^{13}C contact time of 1.5 ms. The spectra were acquired in ca. 34.8 h (red) and 28.2 h (blue) (recycle delay = 10.3 s; 128/64 transients averaged per t_1 point (red/blue) and 95/154 t_1 increments (red/blue)). Relatively unambiguous correlations are specified using dashed lines, and an assignment provided. For the full labelling scheme, see Figure S23, which is the DFT frame.

C. GIPAW DFT and Verification of ANHY

Starting from the crystal structure of **ANHY** determined *via* XRD measurements, geometry optimizations of the H positions were carried out using GIPAW DFT. After H-optimization, the resulting structure was used as input for a magnetic shielding calculation. The outputs of the computations are provided as supplementary files. As there are 50 carbon sites in TENAPANOR, the shift dispersion in the experimental ^{13}C SSNMR spectrum for **ANHY** was insufficient to resolve all ^{13}C sites. However, based upon the peak intensities, a rough judgment of the number of ^{13}C sites at each resonance position in the experimental ^{13}C SSNMR spectra was made. Subsequently, a preliminary (unassigned) ^{13}C shift vs. shielding plot for **ANHY** was generated (Figure S24). It is assumed that the ^{13}C signals of the C-Cl moieties are not observed, due to residual dipolar coupling (RDC)[60,61] between the ^{13}C and $^{35/37}$Cl nuclei. Rather, these signals lie underneath the band of signals in the range from about 126 to 134 ppm. Further details pertaining to the RDCs are provided in the Supporting Information (see Figure S25). A detailed account of the assignment process for **ANHY** is provided in the Supporting Information (see also Figure S26).

A reasonably complete assignment (37 of 50 ^{13}C sites) for **ANHY** was achieved (Table S7), and RMSD values between the DFT-calculated parameter values and those measured experimentally were calculated. While other assignment possibilities for **ANHY** are possible, it would be unlikely that a correct alternative assignment would greatly modify the RMSD. The final (i.e., assigned) shift vs. shielding correlation plots for ^{13}C and ^{1}H are in Figure 7.

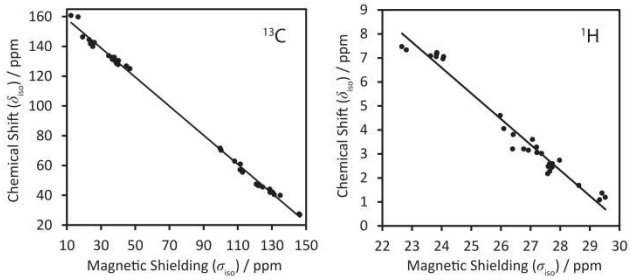

Figure 7. (left) Calculated isotropic ^{13}C magnetic shielding values for 37 assigned carbon (of 50) sites in **ANHY** versus corresponding experimental isotropic ^{13}C chemical shifts. Line of best fit and Pearson product R^2 value: δ_{iso} / ppm = $-0.9758\sigma_{iso}$ / ppm + 168.2; R^2 = 0.9973. (right) Calculated isotropic ^{1}H magnetic shielding values for assigned hydrogen sites in **ANHY** versus experimental isotropic ^{1}H chemical shifts. Line of best fit and Pearson product R^2 value: δ_{iso} / ppm = $-1.0686\sigma_{iso}$ / ppm + 32.24; R^2 = 0.9694.

Using the fit equations in Figure 7, the assigned ^{1}H and ^{13}C RMSD values are calculated to be 0.41 ppm and 2.39 ppm, respectively. A total of 45 ^{1}H shifts (30 unique) attached to 27 carbons were used for the ^{1}H RMSD calculation. Although neither RMSD value is particularly low, both reside within ranges considered acceptable for a valid structure.[62] Hence, the XRD structure for **ANHY** is found to be consistent with the SSNMR and DFT data.

D. Formation Mechanism and Structure of 2HCl

From powder XRD, the crystal structure for **2HCl** was determined to be in an identical space group and to have a similar unit cell size as compared to **ANHY**. Additional powder XRD data were used to solve the structure of **2HCl**, and refinement methods arrived at a satisfactory result (Figure 8 and Figures S27 – S30). With 33 optimisable torsion angles, together with 12 positional and rotational degrees of freedom for the three bodies (diprotonated tenapanor with 2 Cl^{-} ions), it was a major challenge to solve the structure of **2HCl** as described in the Experimental Section. To further verify the structure solution, we performed a CASTEP optimization of the crystal structure while constraining the unit cell parameters as described in the Experimental Section. As will be outlined in more detail, the tenapanor conformation and crystal packing interactions are similar when comparing **ANHY** and **2HCl**. Thus, many NMR chemical shifts would be expected to be very similar, or even identical within measurement precision, for sets of 'analogous' atoms. As part of the characterization process for **2HCl**, solution NMR experiments were performed, which allowed the assignment of the ^{1}H and ^{13}C chemical shifts to sites in the solvated molecule. While there is no reason to expect an exact 1:1 correspondence between the solution data and the solid-state NMR data (*vide infra*), it remains useful to consider. The labelling scheme for the molecule in solution is provided in Figure S1, while the corresponding assigned ^{1}H and ^{13}C chemical shifts are in Table S1.

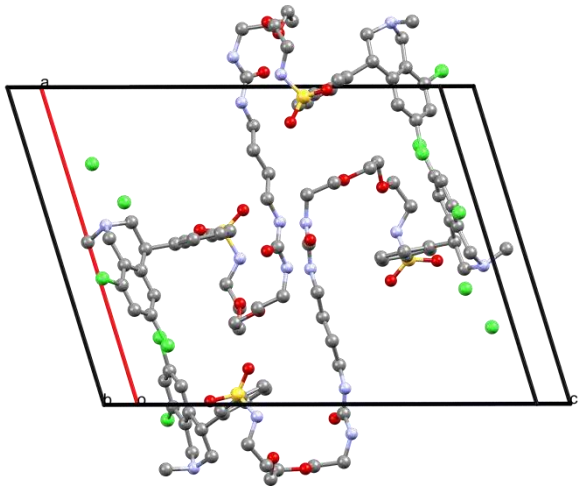

Figure 8. Crystal structure for **2HCl**, determined using synchrotron powder XRD data. Unit cell dimensions: a = 16.4101 Å, b = 8.6105 Å, c = 21.7691 Å, $\alpha = \gamma = 90°$, β = 107.1266°, Z' = 1, Z = 2. H atoms have been omitted for clarity.

By comparing the crystal structures of **ANHY** and **2HCl**, it was realized that most of the main features described above for **ANHY** are also present in **2HCl**. Most importantly, the hydrogen bonding network is similar. The asymmetry in the bifurcated hydrogen bond mode between the urea groups is somewhat more pronounced in **2HCl** compared to **ANHY**. This asymmetry affects the orientation of the above-mentioned phenyl ring, which in **2HCl** is shifted away from interacting with the urea moiety. This is also true for the halogen bonding interaction, which is absent in **2HCl**. The chloride anion forms a salt bridge/hydrogen bond to the protonated nitrogen, but otherwise is hosted in a (surprisingly) non-polar pocket. Overlays of the asymmetric units of the two crystal structures, thus allowing for a direct comparison of the two molecular conformers, establish that they are structurally consonant (heavy atom RMSD = 0.40 Å). As expected, the most significant difference is in the conformation of the methylated dichlorotetrahydroisoquinoline ring (Figure 9) where protonation has occurred. To ensure that the presented structure of **2HCl** solved from the powder data is correct, three additional molecular models differing only in the conformation of the six-membered rings were tested in the structure solution. These attempts resulted in significantly higher χ^2 values, which further increases confidence in the validity of the presented structure.

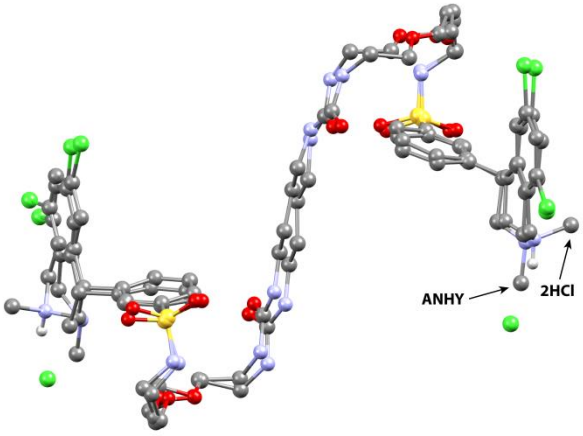

Figure 9. Overlay of the asymmetric units of **ANHY** and **2HCl**. Arrows indicate the methyl position in one of the dichlorotetrahydroisoquinoline rings in each of the two forms. To enhance clarity, all H atoms except those associated with the N atom that is protonated when going from **ANHY** to **2HCl** are omitted.

The difference in ring conformations between **ANHY** and **2HCl** is linked to the ring dynamics in the anhydrous form highlighted earlier. In **ANHY**, the methyl substituent on the nitrogen is positioned equatorially, while in the crystalline **2HCl** form, it is axial. Thus, when forming the **2HCl** salt form, protonation may involve any of several conformers which are in dynamic equilibrium. The protonation will generate two stereocenters at the two nitrogen atoms by attack on the lone-pair from different faces of the dichlorotetrahydroisoquinoline rings. Depending on the nitrogen configuration, *R,R*-, *S,S*-, and *R,S* combinations of the two stereocenters in tenapanor are formed. The ring flip process must also be considered, which gives rise to several conformational possibilities for each stereocenter combination (Figure 10). Protonation of the most stable free form (its major conformation) would result in the *S,S*-configuration at the nitrogen; however, the observed crystalline form of **2HCl** possesses the *R,R*-configuration, which infers generation from the minor conformation. Since there are additional stereocenters at carbon

atoms in tenapanor, protonation at nitrogen gives rise to diastereoisomers which are not interconvertible by ring flips nor by nitrogen inversion. Similar reasoning on the formation of stereoisomeric pairs upon protonation has been provided, for example, in studies on substituted pyridines.[63]

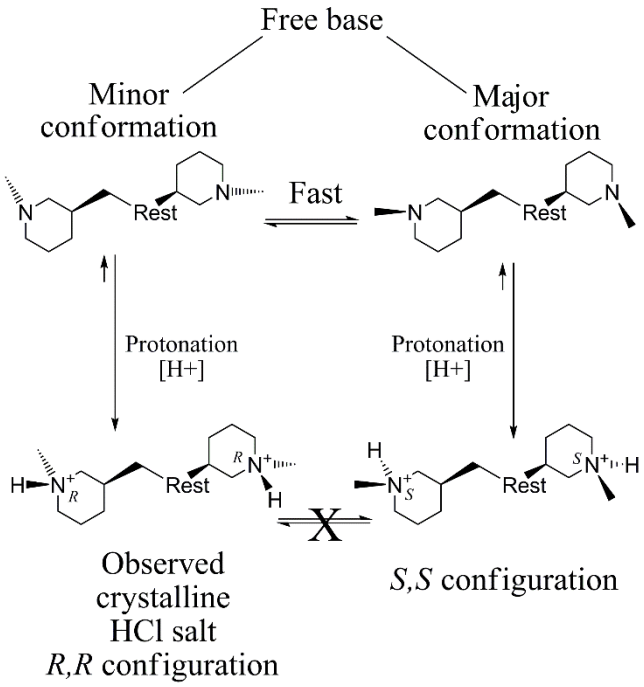

Figure 10. Generation of (*R*,*R*) and (*S*,*S*) diastereoisomers during the formation of HCl salts of several equilibrating free forms of **ANHY**. 'Rest' denotes portions of the tenapanor molecule that are not shown.

Using gas-phase DFT calculations on a model system of **2HCl**, the *S*-diastereoisomer with the methyl group in an equatorial position is predicted to be the most stable molecular conformer of the dichlorotetrahydroisoquinoline ring subsequent to protonation at the nitrogen atom. Specifically, this conformer is found to be 1.2 kcal mol^{-1} more stable than the corresponding *R*-diastereoisomer (i.e. with an axial Me).

As with **ANHY**, various 1D and 2D SSNMR experiments were performed on a sample of **2HCl** to verify the structure determined from powder diffraction data. Unfortunately, the spectral resolution of **2HCl** was low relative to **ANHY**, and several samples of **2HCl** proved to be too unstable to allow experiments under DNP conditions. As a result, a sufficiently complete assignment could not be achieved for **2HCl** and meaningful RMSD calculations could not be performed. The acquired NMR data nevertheless appear consistent with the structure determined using XRD. The vast majority of the SSNMR data and discussion can be found in the Supporting Information (Figures S31 – S44 and Tables S8 – S11); however, a few interesting aspects are now discussed.

From the ^{1}H MAS SSNMR data (Figure S31) there is clear signal intensity at ca. 13 ppm (absent in **ANHY**), which is consistent with formation of R_2N^+-H groups when going from **ANHY** to **2HCl**. Signal intensity in this spectral region is also consistent with the solution NMR data (Table S1). This diagnostic chemical shift is likewise consistent with the value calculated using GIPAW DFT from the **2HCl** crystal structure. Various ^{13}C CP/MAS NMR spectra for **ANHY** and **2HCl** are compared in Figures S37 – S38, with a diagnostic difference being in the region of 55 – 60 ppm, which corresponds to CH_2 group carbons in the urea-like ring system. These signals are distributed over a relatively wide region and are of low intensity in **ANHY**, while they are in a narrower region and have greater intensity in **2HCl**. This is consistent with the notion that **ANHY** is undergoing slow conformational changes, while the conformation in **2HCl** is fixed, at least on the NMR timescale. Further, when comparing the spectra in Figure S38c and S38d, it is likely that CH_3 groups in **ANHY** are near ca. 47 ppm. In contrast, when considering Figures S38a and S38b, the most probable resonance positions for the Me groups in **2HCl** are in the 37 – 40 ppm region. This establishes a significant ^{13}C shift difference in these chemical sites of **ANHY** and **2HCl** of ca. 8 ppm, which is consistent with the structural change (i.e., ring-flip and inversion process) noted earlier. The most convincing SSNMR data for the protonation site locations comes from the ^{15}N CP/MAS spectra. For **2HCl**, 6 resonances are resolved (Figure 11a), but the signal intensities are distributed in a 1:1:2:1:1:2 fashion. After protonation, the ^{1}H-^{15}N CP/MAS dynamics would be expected to be relatively more similar across the nitrogen sites in **2HCl**, in agreement with observations. There is also a large ^{15}N chemical shift difference when comparing the ^{15}N NMR signals associated with the ring nitrogen nuclei in **2HCl** and **ANHY** (Figure 11).

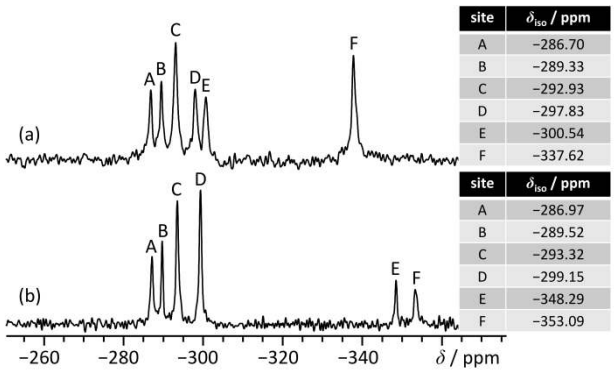

site	δ_{iso} / ppm
A	−286.70
B	−289.33
C	−292.93
D	−297.83
E	−300.54
F	−337.62

site	δ_{iso} / ppm
A	−286.97
B	−289.52
C	−293.32
D	−299.15
E	−348.29
F	−353.09

Figure 11. ^{15}N CP/MAS NMR spectra acquired at B_0 = 16.4 T, using ν_{MAS} = 6.8 kHz for **2HCl** (a) and ν_{MAS} = 6.0 kHz for **ANHY** (b). The spectrum in (a) resulted from 16384 scans, while (b) resulted from 14424 scans. Observed δ_{iso}(^{15}N) values are provided to the right of each spectrum.

E. Crystal Structure Prediction (CSP)

To further evaluate the polymorphic landscape of **2HCl**, different molecular diastereoisomeric conformers with combinations of nitrogen stereochemistry and ring conformation (with the methyl group in the axial or the equatorial position) were created. The polymorph landscape associated with each of the different diastereoisomers of **2HCl** (operating under the assumption of rigid conformers once within the crystalline lattice) were analyzed by first testing whether the in-house developed SSPT force-field would be able to reproduce the structure determined by XRD. Gratifyingly, the cell parameters and atomic positions observed experimentally were reproduced by the computational method (Figure S45, $RMSD_{30}$ = 0.523 Å; volume difference <

6%). This therefore gives confidence that the SSPT force-field would give reliable polymorph landscapes for other diastereoisomers. Similarly, the CSP methodology was tested for **ANHY**, yielding an $RMSD_{30} = 0.136$ Å and a volume difference < 1% when comparing the most stable predicted structure to the scXRD structure (Figure S46).

In total, 300 diastereoisomeric **2HCl** crystal structures were generated and optimized using the SSPT force-field. The 60 most stable, as evaluated by comparing force-field energies, were selected for dispersion-corrected DFT (DFT-D) energy calculations and thus a stability re-ranking. The 20 most stable crystal structures of these were then selected for further DFT-D optimization using GIPAW DFT and from these the eight most stable structures were selected for final NMR calculations. By this approach we have the possibility to study the impact of the nitrogen stereochemistry and ring conformations on the NMR chemical shifts.

F. An Amorphous Form of 2HCl

For the different diastereoisomers described above, we wanted in particular to see if calculated properties could provide any structural details on amorphous **2HCl** (**a-2HCl**) forms. From the calculated ^{13}C chemical shifts of the methyl group attached to the nitrogen in the dichlorotetrahydroisoquinoline ring, we expect a clearly distinguishable difference between structures where the methyl was in the axial or equatorial position. Specifically, for the CSP-generated diastereoisomeric crystal structures described above, with the methyl group in the axial position the isotropic ^{13}C shift varied between 33.1 – 39.1 ppm, while if the methyl was in the equatorial position, this shift varied between 39.6 – 43.1 ppm. Thus, **2HCl**, with methyl groups in the axial position, should display lower Me group chemical shift values relative to **ANHY**. For **a-2HCl**, while a mixture of both conformers should be anticipated, mainly equatorial methyl groups are expected. As such, a distribution towards higher chemical shift values should be observed. Experimentally, the methyl shift is observed at 37.1-37.2 ppm in crystalline **2HCl**. Gratifyingly, in **a-2HCl**, an increased relative shift is observed with the highest intensity in the region 42.5-43.5 ppm (Figure 12). This provides evidence that the amorphous form is composed of a mixture of conformations but this shift change indicates that **a-2HCl** consists mainly of ring conformations with equatorial methyl groups which originates from protonation of the major conformer, as observed in **ANHY**.

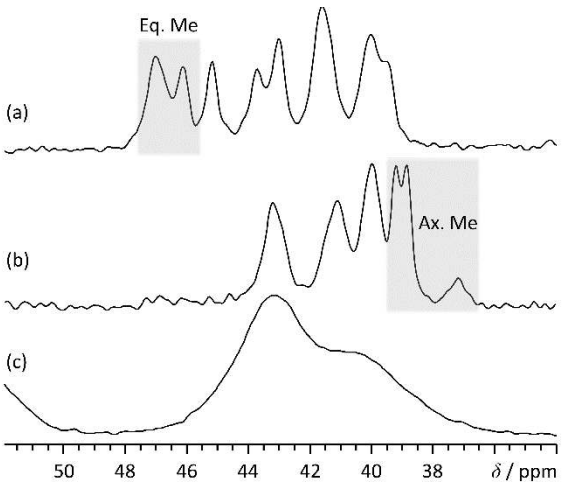

Figure 12. Extracts from ^{13}C CP/MAS NMR spectra at $B_0 = 9.4$ T, highlighting the chemical shifts associated with methyl group carbons (grey shading) for **ANHY** (a), **2HCl** (b), and **a-2HCl** (c).

G. Amorphous Form Stability

Compared to **ANHY**, **a-2HCl**, which does not possess long-range order, displayed superior bioavailability in the first clinical studies as a consequence of its higher kinetic aqueous solubility (Figure 13). As the diastereoisomers of the HCl salt are not interconvertible, and as crystalline **2HCl** is formed from a minor conformer of the dichlorotetrahydroisoquinoline ring, a possible route to prevent **a-2HCl** from crystallizing into **2HCl** appears to be available. Suggested reaction conditions to enable this control are here described. By ensuring that the pH is well below 2 (pK_a of **ANHY**= 3.70), all the equilibrating dichlorotetrahydroisoquinoline ring conformers will be protonated, and thus a mixture of diastereoisomers of the salt of the protonated **ANHY** should be formed in solution. If the pH is increased, the equilibrium between the free form and the salt will be shifted, and a portion of the free base will be formed (Figures 10 and 13). This will lead to conditions such that the dichlorotetrahydroisoquinoline ring conformers are again in dynamic equilibrium. The conformer which results in the *R,R*-diastereoisomer, which is observed in crystalline **2HCl**, upon protonation will then be formed to some extent (Figure 10). The amorphous salt form is observed at low pH. By controlling the solution pH, the driving force to crystallize the *R,R*-diastereoisomer can thus be altered, which is therefore also a way of controlling the amorphosity of the HCl salt of tenapanor.

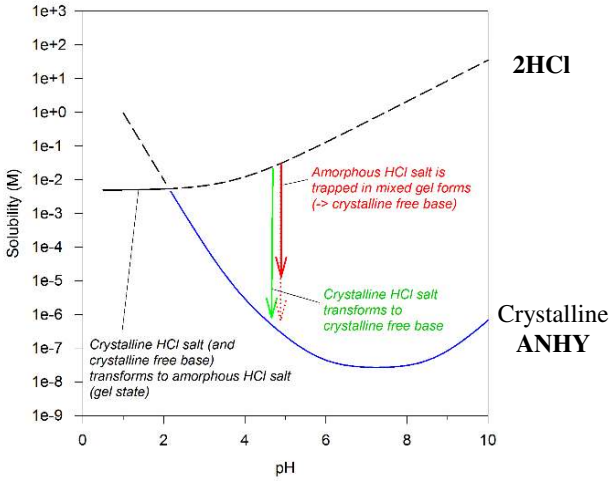

Figure 13. Aqueous solubility dependency of various tenapanor -containing systems as a function of the pH.

Conclusions

Using a variety of complementary techniques, including powder and single-crystal X-ray diffraction, solution- and solid-state NMR, crystal structure predictions, and quantum chemical (QM) calculations, we have determined the crystal structures for two systems containing the unusually large tenapanor drug molecule. NMR crystallography techniques were used to assign and validate the crystal structure of one form of the free base (**ANHY**). Use of dynamic nuclear polarization (DNP) methods

were indispensable, as they afforded order-of-magnitude gains in sensitivity. Thus, data from very challenging and insensitive experiments (e.g., ^{13}C-^{13}C INADEQUATE) could be used to greatly enhance the assignment process, which is a critical step during NMR crystallography structure validation. Incompatibilities of the **2HCl** system with various DNP radical solvents precluded the use of DNP for this system, but after comparing experimental and GIPAW DFT-computed chemical shifts, it was found that the NMR data were largely consistent with the **2HCl** diffraction structure. From the structural analysis of the resolved structures of both **ANHY** and **2HCl** we observe conformational differences in the dichlorotetrahydroisoquinoline rings which has consequences for the relative orientation of the methyl group on the ring nitrogen. In the crystal structure of **ANHY** the methyl group is oriented in an equatorial position while in the crystal structure of **2HCl** it is oriented in an axial position. From QM-calculations we predict fast equilibrium dynamics to take place between these different ring conformations in solution. Protonation of tenapanor using HCl generates a dichloride salt of which the crystalline material **2HCl** originates from the minor of these conformations. To be able to drive all of tenapanor into this diastereoisomeric crystal form, one must therefore involve the equilibrium between axial (minor) and equatorial (major) conformations of **ANHY** in solution, thus by nitrogen deprotonation. By keeping the pH well below the pK_a of **ANHY** the equilibrium between **ANHY** and **2HCl** can thus be controlled. By this mechanism the crystallization of **2HCl** can be avoided and the amorphous form **a-2HCl** of the dichloride salt is thus stabilized.

ASSOCIATED CONTENT

Supporting Information: Solution ^{1}H and ^{13}C spectra, additional ^{1}H, ^{13}C, ^{15}N SSNMR spectra, $^{1}H(T_1)$ measurements, assignment details, ^{13}C–^{13}C MAT NMR spectra, DFT-calculated system energies and Cartesian coordinates, structural overlays of CSP and experimental crystal structures. This material is available free of charge via the Internet at http://pubs.acs.org.

AUTHOR INFORMATION

Corresponding Authors

* Sten Nilsson Lill, sten.nilsson-lill@astrazeneca.com ORCID ID: 0000-0003-4818-8084; Lyndon Emsley, lyndon.emsley@epfl.ch

Present Addresses

† Department of Chemistry, Oakland University, 48309, Rochester, MI, United States of America.

Author Contributions

The manuscript was written through contributions of all authors. All authors have given approval to the final version of the manuscript.

Funding Sources

This research was funded by AstraZeneca.

Disclosures

SONL, AP, ASA, ML, PA, SG and SS are employees at AstraZeneca. All authors declare no competing financial interest.

ACKNOWLEDGMENT

CMW would like to acknowledge NSERC for a postdoctoral fellowship. Mark E. Light at the University of Southampton is acknowledged for work on determining the structure of **ANHY** using single-crystal X-ray diffraction data.

ABBREVIATIONS

IBS-C, irritable bowel syndrome with constipation; ESRD, end-stage renal disease; GI, gastrointestinal; scXRD, single-crystal X-ray diffraction; NMR, nuclear magnetic resonance; DFT, density functional theory; SSNMR, solid-state NMR; CSP, crystal structure predictions; RMSD, root-mean-squared deviation; MAS, magic angle spinning; CP, cross-polarization; DNP, dynamical nuclear polarization; CASTEP, Cambridge Serial Total Energy Package; GGA, generalized gradient approximation; XC, exchange-correlation; PBE, Perdew-Burke- Ernzerhof; TS, Tkatchcnko-Scheffler; SCF, self-consistent field; SSPT, solid state prediction tool; MC, Monte-Carlo; PXRD, powder X-ray diffraction; HETCOR, heteronuclear correlation; MAT, magic-angle turning

Graphical Abstract

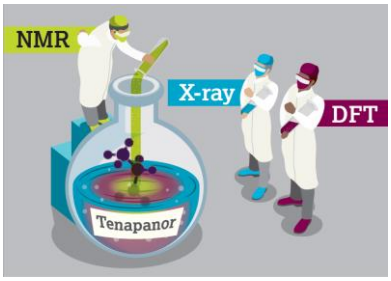

References

(1) Vippagunta, S. R.; Brittain, H. G.; Grant, D. J. W. *Advanced Drug Delivery Reviews* **2001**, *48*, 3.
(2) Hancock, B. C.; Zografi, G. *Journal of Pharmaceutical Sciences* **1997**, *86*, 1.
(3) Baghel, S.; Cathcart, H.; O'Reilly, N. J. *Journal of Pharmaceutical Sciences* **2016**, *105*, 2527.
(4) Vehring, R. *Pharmaceutical Research* **2008**, *25*, 999.
(5) Chey, W. D.; Lembo, A. J.; Rosenbaum, D. P. *Am J Gastroenterol* **2017**, *112*, 763.
(6) Spencer, A. G.; Labonte, E. D.; Rosenbaum, D. P.; Plato, C. F.; Carreras, C. W.; Leadbetter, M. R.; Kozuka, K.; Kohler, J.; Koo-McCoy, S.; He, L.; Bell, N.; Tabora, J.; Joly, K. M.; Navre, M.; Jacobs, J. W.; Charmot, D. *Science Translational Medicine* **2014**, *6*, 227ra36.
(7) Shankland, K.; Spillman, M. J.; Kabova, E. A.; Edgeley, D. S.; Shankland, N. *Acta Crystallographica Section C* **2013**, *69*, 1251.
(8) Baias, M.; Dumez, J.-N.; Svensson, P. H.; Schantz, S.; Day, G. M.; Emsley, L. *Journal of the American Chemical Society* **2013**, *135*, 17501.
(9) Nilsson Lill, S. O.; Schantz, S.; Broo, V.; Broo, A. In *Computational Pharmaceutical Solid State Chemistry* Abramov, Y., Ed.; Wiley: **2016**, p 145.
(10) Nilsson Lill, S. O.; Broo, A. *Crystal Growth & Design* **2014**, *14*, 3704.
(11) Falcicchio, A.; Nilsson Lill, S. O.; Perna, F. M.; Salomone, A.; Coppi, D. I.; Cuocci, C.; Stalke, D.; Capriati, V. *Dalton Transactions* **2015**, *44*, 19447.
(12) Thurber, K. R.; Robert, T. *J. Magn. Reson.* **2009**, *196*, 84.
(13) Hayashi, S.; Hayamizu, K. *Bull. Chem. Soc. Jpn.* **1991**, *64*, 688.
(14) Maly, T.; Debelouchina, G. T.; Bajaj, V. S.; Hu, K.-N.; Joo, C.-G.; Mak-Jurkauskas, M. L.; Sirigiri, J. R.; van der Wel, P. C. A.; Herzfeld, J.; Temkin, R. J.; Griffin, R. G. *J. Chem. Phys.* **2008**, *128*, 052211.
(15) Ni, Q. Z.; Daviso, E.; Can, T. V.; Markhasin, E.; Jawla, S. K.; Swager, T. M.; Temkin, R. J.; Herzfeld, J.; Griffin, R. G. *Acc. Chem. Res.* **2013**, *46*, 1933.
(16) Rossini, A. J.; Zagdoun, A.; Lelli, M.; Lesage, A.; Coperét, C.; Emsley, L. *Acc. Chem. Res.* **2013**, *46,* 1942.
(17) Smith, A. N.; Long, J. R. *Anal. Chem.* **2016**, *88*, 122.
(18) Sauvée, C.; Rosay, M.; Casano, G.; Aussenac, F.; Weber, R. T.; Ouari, O.; Tordo, P. *Angew. Chem. Int. Ed.* **2013**, *52*, 10858.
(19) Rossini, A. J.; Emsley, L.; O'Dell, L. A. *Phys. Chem. Chem. Phys.* **2014**, *16*, 12890.
(20) Kubicki, D. J.; Rossini, A. J.; Purea, A.; Zagdoun, A.; Ouari, O.; Tordo, P.; Engelke, F.; Lesage, A.; Emsley, L. *J. Am. Chem. Soc.* **2014**, *136*, 15711.
(21) Mentink-Vigier, F.; Paul, S.; Lee, D.; Feintuch, A.; Hediger, S.; Vega, S.; De Paëpe, G. *Phys. Chem. Chem. Phys.* **2015**, *17*, 21824.
(22) Clark, S. J.; Segall, M. D.; Pickard, C. J.; Hasnip, P. J.; Probert, M. I. J.; Refson, K.; Payne, M. C. *Z. Kristallogr.* **2005**, *220*, 567.
(23) Pickard, C. J.; Mauri, F. *Phys. Rev. B* **2001**, *63*, 245101.
(24) Yates, J. R.; Pickard, C. J.; Mauri, F. *Phys. Rev. B* **2007**, *76*, 024401.
(25) Perdew, J. P.; Burke, K.; Ernzerhof, M. *Phys. Rev. Lett.* **1996**, *77*, 3865.
(26) Perdew, J. P.; Burke, K.; Ernzerhof, M. *Phys. Rev. Lett.* **1997**, *78*, 1396.
(27) Baias, M.; Widdifield, C. M.; Dumez, J.-N.; Thompson, H. P. G.; Cooper, T. G.; Salager, E.; Bassil, S.; Stein, R. S.; Lesage, A.; Day, G. M.; Emsley, L. *Phys. Chem. Chem. Phys.* **2013**, *15*, 8069.
(28) Kerr, H. E.; Mason, H. E.; Sparkes, H. A.; Hodgkinson, P. *CrystEngComm* **2016**, *18*, 6700.
(29) Tkatchenko, A.; Scheffler, M. *Phys. Rev. Lett.* **2009**, *102*, 073005.
(30) Briggner, L.-E.; Hendrickx, R.; Kloo, L.; Rosdahl, J.; Svensson, P. H. *ChemMedChem* **2011**, *6*, 60.
(31) Briggner, L.-E.; Kloo, L.; Rosdahl, J.; Svensson, P. H. *ChemMedChem* **2014**, *9*, 724.
(32) Neumann, M. A.; Leusen, F. J. J.; Kendrick, J. *Angewandte Chemie* **2008**, *120*, 2461.
(33) Shivakumar, D.; Harder, E.; Damm, W.; Friesner, R. A.; Sherman, W. *Journal of Chemical Theory and Computation* **2012**, *8*, 2553.
(34) Grimme, S. *Journal of Computational Chemistry* **2006**, *27*, 1787.
(35) Sturniolo, S.; Green, T. F. G.; Hanson, R. M.; Zilka, M.; Refson, K.; Hodgkinson, P.; Brown, S. P.; Yates, J. R. *Solid State Nuclear Magnetic Resonance* **2016**, *78*, 64.
(36) Zhao, Y.; Truhlar, D. G. *Theoretical Chemistry Accounts* **2008**, *120*, 215.
(37) Schrodinger Inc., LLC: New York, **2013**.
(38) Zhao, Y.; Truhlar, D. G. *Accounts of Chemical Research* **2008**, *41,* 157.
(39) David, W. I. F.; Shankland, K.; van de Streek, J.; Pidcock, E.; Motherwell, W. D. S.; Cole, J. C. *Journal of Applied Crystallography* **2006**, *39*, 910.
(40) van de Streek, J.; Neumann, M. A. *Acta Crystallographica Section B* **2010**, *66*, 544.
(41) Rigaku/MSC: The Woodlands, TX: **2005**.
(42) V1.171.37.35 ed.; Oxford Diffraction /Agilent Technologies UK Ltd, Yarnton, England.: **2014**.
(43) Sheldrick, G. *Acta Crystallographica Section A* **2008**, *64*, 112.
(44) Sheldrick, G.; University of Göttingen, Germany: **2012**.
(45) Bondi, A. *The Journal of Physical Chemistry* b, *68*, 441.
(46) Widdifield, C. M.; Nilsson Lill, S. O.; Broo, A.; Lindkvist, M.; Pettersen, A.; Svensk Ankarberg, A.; Aldred, P.; Schantz, S.; Emsley, L. *Physical Chemistry Chemical Physics* **2017**, *19*, 16650.
(47) Widdifield, C. M.; Robson, H.; Hodgkinson, P. *Chemical Communications* **2016**, *52*, 6685.
(48) Martineau, C.; Senker, J.; Taulelle, F. In *Annual Reports on NMR Spectroscopy*; Webb, G. A., Ed.; Academic Press: **2014**; Vol. *82*, p 1.
(49) Ashbrook, S. E.; McKay, D. *Chemical Communications* **2016**, *52*, 7186.
(50) Xu, Y.; Southern, S. A.; Szell, P. M. J.; Bryce, D. L. *CrystEngComm* **2016**, *18*, 5236.
(51) Bryce, D. *IUCrJ* **2017**, *4*, 350.

(52) Harris, R. K.; Wasylishen, R. E.; Duer, M. J. *NMR crystallography*; Wiley, **2009**.
(53) Wu, X. L.; Burns, S. T.; Zilm, K. W. *Journal of Magnetic Resonance, Series A* **1994**, *111*, 29.
(54) Gan, Z. *Journal of the American Chemical Society* **1992**, *114*, 8307.
(55) Hu, J. Z.; Alderman, D. W.; Ye, C. H.; Pugmire, R. J.; Grant, D. M. *Journal of Magnetic Resonance, Series A* **1993**, *105*, 82.
(56) Gann, S. L.; Baltisberger, J. H.; Pines, A. *Chemical Physics Letters* **1993**, *210*, 405.
(57) Lesage, A.; Auger, C.; Caldarelli, S.; Emsley, L. *Journal of the American Chemical Society* **1997**, *119*, 7867.
(58) Lesage, A.; Bardet, M.; Emsley, L. *Journal of the American Chemical Society* **1999**, *121*, 10987.
(59) Widdifield, C. M.; Schurko, R. W. *Concepts in Magnetic Resonance Part A* **2009**, *34A*, 91.
(60) Kaplan, S.; Pines, A.; Griffin, R. G.; Waugh, J. S. *Chemical Physics Letters* **1974**, *25*, 78.
(61) Griffin, R. G.; Pines, A.; Waugh, J. S. *The Journal of Chemical Physics* **1975**, *63*, 3676.
(62) Widdifield, C. M.; Robson, H.; Hodgkinson, P. *Chem. Commun.* **2016**, *52*, 6685.
(63) Kolocouris, A.; Outeiriño, J. G.; Anderson, J. E.; Fytas, G.; Foscolos, G. B.; Kolocouris, N. *J. Org. Chem.* **2001**, *66*, 4989.